Magneto-optical properties of carbon toroids: Influence of geometry and magnetic field

Feng-Lin Shyu
Department of Physics, Chinese Military Academy, Kaohsiung, Taiwan 830, Republic of China
(Received 2 February 2005; revised manuscript received 21 March 2005; published 14 July 2005)

Magneto-optical excitations of carbon toroids by the cross polarized light are studied within the gradient approximation. Their dependences on the magnitude (ϕ) and the direction (α) of the magnetic field vary with the changes in the toroid geometry (chiral angle, height, and radius). The absorption spectra of armchair toroids are hardly affected by ϕ and α. In contrast, the absorption peaks of zigzag toroids, due to the changes in the energy spacing and the destruction of the state degeneracy, obviously split and shift as ϕ and α vary. For different α's, the threshold excitation energy (ω_{th}) displays the periodic Aharonov-Bohm oscillations or monotonously decreases as ϕ increases. Moreover, the ϕ dependences of ω_{th} on the toroid height and the toroid radius are significantly different.

DOI: 10.1103/PhysRevB.72.045424 PACS number(s): 78.67.−n, 73.61.Wp, 71.15.Ap

The very considerable potential of carbon nanotubes (CNs) for nanotechnology has stirred many studies since they were discovered in 1991 by Iijima.[1] Theoretical predictions showed that a carbon nanotube can be either metallic or semiconducting, and that this strongly depends on its geometric structure. Electronic properties have been also confirmed by scanning tunneling microscopy. A carbon toroid (CT) is a form of carbon structure, which was formed by knitting the open two ends of a CN and was discovered by Liu *et al.*[2] Because its average radius is much larger than its height or width, a CT is very thin.

This new quasi-zero-dimensional system has prompted many investigations, such as geometric structures,[2–8] electronic structures,[9–14] magnetic properties,[15–21] optical properties,[22,23] electronic excitations,[24,25] thermal properties,[26] and transport properties.[27,28] The low-temperature magnetoresistance of CTs has been observed experimentally,[28] and predicted to be used to make interference devices. On the other hand, electronic structures of CTs, at zero field, have been calculated within the tight-binding model, which included the curvature effect. The evaluated band structures predicted four types of energy gaps, which are very sensitive to the changes in the geometric structure.[9,10] The tight-binding model has been further used to evaluate the magnetoelectronic structures for CTs[14] and CNs.[29] Consequently, the magnetoband structure, the energy gap, the energy spacing, and the state degeneracy strongly depend on the magnitude and the direction of the magnetic field. A CT is similar to a CN in geometric structure in that they both have a cylindrical symmetry. The magnetic field (B) is thus expected to play an important role on the induced quantum effects. Experimentally, due to their larger radius, CTs are more suitable than CNs in helping to identify the quantum effects induced by the magnetic field.

In this work, we use the tight-binding model to calculate the magnetoelectronic states. Then magneto-optical excitations of CTs in the presence of cross polarized light are evaluated within the gradient approximation.[17,30–35] Similar approximations have been successfully applied to understand the optical spectra of graphite[30] and carbon nanotubes.[17,31–35] In the calculation, the curvature effect is included and Zeeman splitting is negligible because of the large CTs. Our study shows that the magnetic field could cause a large shift in the longitudinal angular momentum (L) and strong coupling of different L's. Furthermore, it would significantly induce the changes of the energy spacing, the quantization of the wave function, and the destruction of the state degeneracy. Such changes depend strongly on the toroid geometry [radius (R), height ($2r$), and chiral angle (θ)]. They are directly reflected in the optical excitations, such as the optical spectral function $A(\omega)$ and the threshold excitation energy ω_{th}. The predicted results could be verified by the experimental measurements, as was done for carbon nanotubes.[36–41]

A carbon toroid is a rolled-up graphite sheet such that the carbon atom at the origin coincides with the two atoms at $\mathbf{R_x}=m\mathbf{a_1}+n\mathbf{a_2}$ and $\mathbf{R_y}=p\mathbf{a_1}+q\mathbf{a_2}$ simultaneously (see details in Fig. 1 of Ref. 9), where $\mathbf{a_1}$ and $\mathbf{a_2}$ are the primitive lattice vectors of the graphite sheet. The parameters (m,n,p,q) define a carbon toroid. The radius, the height, and the chiral angle are, respectively, $R=b\sqrt{3(p^2+pq+q^2)}/2\pi$, $2r=b\sqrt{3(m^2+mn+n^2)}/\pi$, and $\theta=\tan^{-1}-[\sqrt{3}n/(2m+n)]$. $b=1.42$ Å is the C-C bond length.

In the absence of magnetic field, the π-electron states of a CT are derived from those of a graphite sheet, but with the periodic boundary conditions along the transverse ($\hat{x}$) and the longitudinal ($\hat{y}$) directions taken into account. The discrete energy states are characterized by the transverse ($J=1,2,\ldots N_u$) and the longitudinal ($L=1,2,\ldots N_v$) angular momenta. $N_u=2\sqrt{(m^2+mn+n^2)(p^2+pq+q^2)}/3/N_v$, and N_v is the double of the maximum common factor of (p,q). The curvature effect, the misorientation of the $2p_z$ orbital on the cylindrical surface, is also included in the calculations. It affects the nearest-neighbor interaction of the A and B atoms. The resonance integrals along the different nearest-neighbor directions are, respectively, given by $\gamma_1=\gamma_0(1-b^2\sin^2\theta/8r^2)$, $\gamma_2=\gamma_0[1-b^2(\sin\theta+\sqrt{3}\cos\theta)^2/32r^2]$, and $\gamma_3=\gamma_0[1-b^2(\sin\theta-\sqrt{3}\cos\theta)^2/32r^2]$.[42] $\gamma_0(\sim 2.6-3$ eV) (Refs. 14, 21, and 29) is the nearest-neighbor interaction without the curvature effect between the A and B atoms.

The magnetic field is $\mathbf{B}=B\cos\alpha\hat{z}+B\sin\alpha\hat{R}=B_{\|}\hat{z}+B_{\perp}\hat{R}$ and the magnetic flux is $\phi=\pi R^2B$. α is the angle between

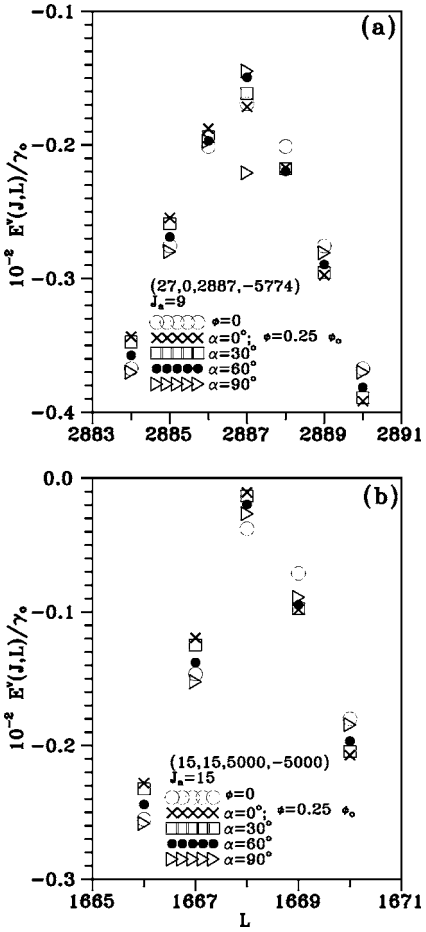

FIG. 1. Low-energy magnetoelectronic states at $\phi=0.25\ \phi_0$ and different field directions are shown for (a) the (27,0,2887, −5774) toroid of ($J_a=9$, $L=2884-2890$) and (b) the (15,15,5000, −5000) toroid of ($J_a=15$, $L=1666-1670$). Those at zero flux are also shown for comparison.

the magnetic field and the symmetric axis ($\hat{z}$). It is convenient to use the cylindrical coordinates $(R,\Omega,z)(\hat{y}\|\hat{\Omega};\Omega=y/R)$. The vector potential is $\mathbf{A}=RB\cos\alpha/2\hat{\Omega}+RB\sin\alpha\sin\Omega\hat{z}$. It induces a magnetic phase factor $G=\int\mathbf{A}(\mathbf{D})\cdot d\mathbf{D}$. The effect of the magnetic field on J is negligible because of $R\gg 100r$. $B_\parallel$ makes L change into $L+\phi\cos\alpha/\phi_0$, and $B_\perp$ leads to the coupling of different L's. $\phi_0(=hc/e)$ is the fundamental magnetic flux. The calculations due to $B_\perp$ are relatively complicated, since each wave function is the superposition of those of different L's. The Hamiltonian matrix in the presence of $B_\perp$ needs to be expanded in the tight-binding functions of the L space. It is characterized by a $2N_v\times 2N_v$ Hermitian matrix.[14,21] Electronic states are obtained by diagonalizing the Hamiltonian matrix. The state energy is $E^h(J,\phi,\alpha)$, where $h=v(c)$ represents the $\pi(\pi^*)$ state with negative (positive) energy. The Zeeman splitting energy $E_z=g\sigma\phi/m^*R^2\phi_0$. $g\approx 2$ is the same as that of pure graphite. $\sigma=\pm 1/2$ is the electron spin and m^* is the bare electron mass. It could be neglected except at very large $\phi(\sim 10^2\phi_0)$. The total energy is $E^h(J,\phi,\alpha;\sigma)=E^h(J,\phi,\alpha)+E_z$. CTs might have an energy gap between the highest occupied molecular orbital (HOMO) and the lowest unoccupied molecular orbital (LUMO). The features of calculated electronic states will be directly reflected in the optical excitations.

The CTs are assumed to be excited by an EM field with an electric polarization $\mathbf{E}_\perp$ perpendicular to the symmetric axis. The low-frequency optical excitations depend on the dipole transition matrix element, $\langle\Psi^{h'}(J,L';\phi)|\cos\beta\,P_\beta/m_e|\Psi^h\times(J,L;\phi)\rangle$. β is the angle between $\mathbf{E}_\perp$ and $\mathbf{P}$ (momentum). The selection rule is $L'=L\pm 1$. The absorption spectrum is evaluated within the gradient approximation. The spectral function is given by the Fermi golden rule,[43]

$$A(\omega)=\frac{e^2}{\pi^2r^2R}\sum_{h,h',J,L}|\langle\Psi^{h'}(J,L\pm 1;\phi)|\frac{e^{\pm i\beta}P_\beta}{m_e}|\Psi^h(J,L;\phi)\rangle|^2\mathrm{Im}\left\{\frac{f[E^h(J,L;\phi)]-f[E^{h'}(J,L\pm 1;\phi)]}{E^{h'}(J,L\pm 1;\phi)-E^h(J,L;\phi)-\omega-i\Gamma}\right\}. \quad (1)$$

$\Gamma=5\times 10^{-5}\ \gamma_0$ is the energy width due to various deexcitation mechanisms.

The zigzag (27,0,2887, −5774) CT ($\theta=0°$, $R=1957$ Å, and $2r=21.1$ Å) and the armchair (15,15,5000, −5000) CT ($\theta=-30°$, $R=1957$ Å, and $2r=20.3$ Å) are chosen as model studies. As a result of the longitudinal and transverse boundary conditions, they have many discrete electronic states. The low-energy states of the zigzag CT are shown in Fig. 1(a). The occupied states are symmetric to the unoccupied states around the Fermi level $E_F=0$. At $\phi=0$, a zigzag CT has fourfold degeneracy except for the doubly degenerate HOMO and LUMO. The fourfold and double degeneracies, respectively, come from $E(J,L)=E(J,N_v-L)=E(N_u-J,L+N_v/2)=E(N_u-J,N_v/2-L)$ and $E(J_a,L_a)=E(N_u-J_a,L_a+N_v/2)$. (J_a,L_a) represents the HOMO nearest to the Fermi level. The effects of the parallel magnetic field on angular momenta L and N_v-L are different, e.g., E^v at $\alpha=0°$ and $\phi=0.25\ \phi_0$. Consequently, the fourfold degeneracy is changed into a double degeneracy, but the double degeneracy from HOMO and LUMO remains unchanged. When the magnetic field deviates from the toroid axis, $B_\perp$ induces the coupling of different L's in addition to the shift of L from $B_\parallel$. Each electronic state consists of different L's. Each state could be characterized by a specific L with the maximum probability. The coupling of L's is strong only at large ϕ and α. At $\phi=0.25\ \phi_0$, this coupling hardly affects the state de-

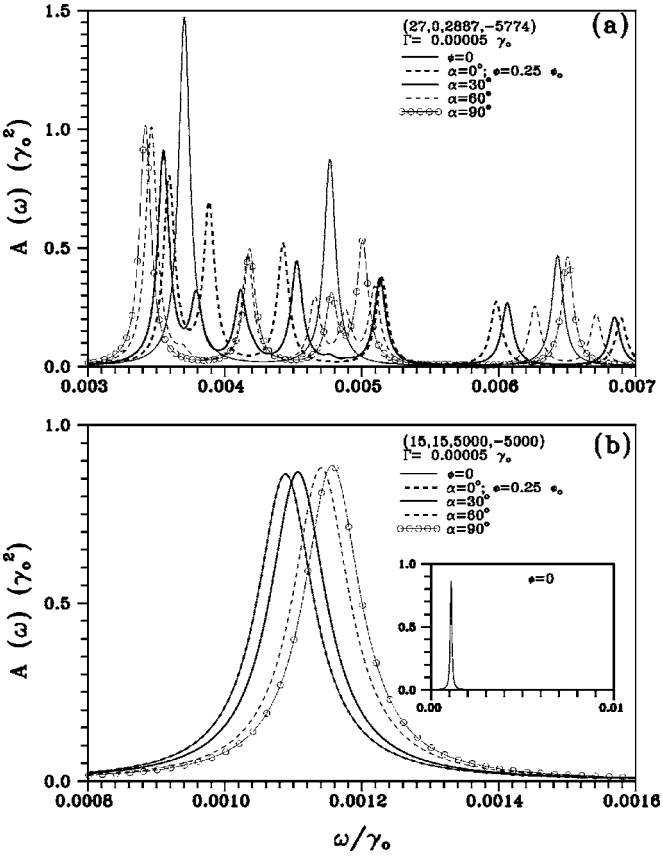

FIG. 2. Absorption spectra are calculated at $\phi=0.25\ \phi_0$ and different α's for the (a) (27,0,2887, −5774) and (b) (15,15,5000, −5000) toroids. Also shown for comparison are results without magnetic flux.

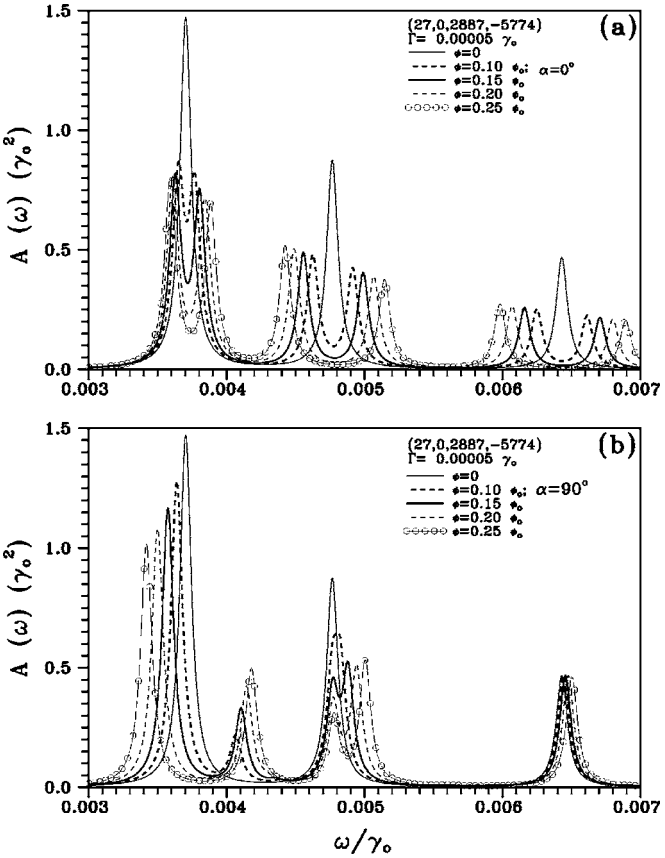

FIG. 3. Similar plot as Fig. 2, but shown for the (27,0,2887, −5774) toroid at (a) $\alpha=0°$ and (b) $\alpha=90°$, and different ϕ's

generacy even at $\alpha=90°$, but the energy spacing between states closer to Fermi level is apparently changed. An energy gap comes from the ($J_a=9$, $L_a=2887$) or ($J_a=18$, $L_a=5774$) states for any α.

The electronic states of an armchair CT are very different from those of a zigzag CT. The former, as shown in Fig. 1(b), has a smaller energy gap because of the weaker curvature effect. At $\phi=0$, an armchair CT has double degeneracy, i.e., $E(J,L)=E(J,N_v-L)$. At $\alpha\neq 90°$ and $\phi=0.25\ \phi_0$, the double degeneracy is destroyed. The $L=1668$ state approaches the Fermi level. An energy gap is only associated with the ($J_a=15$, $L_a=1668$) state, not the ($J_a=15$, $L_a=8332$) state. At large ϕ and α, this coupling has an effect on the HOMO and the state degeneracy. It is remarkable that all of the states have no degeneracy at $\alpha\neq 90°$ for different ϕ's. The state degeneracy at $\alpha=90°$ is recovered to the $\phi=0$ case.

At zero temperature, electrons are excited from the occupied π states to the unoccupied π^* states. The inter-π-state excitations play the main role in the absorption spectra, as shown in Fig. 2. For a zigzag CT, Fig. 2(a) shows that the intensity of $A(\omega)$ declines with increasing frequency at $\phi=0$. At $\phi=0.25\ \phi_0$, the destruction of state degeneracy induces the splitting of absorption peaks, thus the peak height is reduced. In addition, the change in energy spacing causes the absorption peak shifts. ω_{th}, which is related to the highest absorption peak, decreases with an increase in α. Compared with the zigzag CT, an armchair CT only exhibits the lowest-frequency inter-π-state excitation [see inset in Fig. 2(b)] at $\phi=0$. The other excitation channels hardly exist due to the vanishing dipole matrix element. This is because of the intrinsic symmetry of the geometric structure. At $\phi=0.25\ \phi_0$ and $\alpha=0°$, the absorption spectrum [Fig. 2(b)] is almost the same as in the $\phi=0$ case. At $\alpha\neq 0°$, the coupling of L could induce other excitation channels and thus absorption peaks (not shown here). But their intensity is too weak to be measured by experiments. On the other hand, the intensity and position of the absorption peak associated with ω_{th} are slightly changed. Such results show that the optical excitations of armchair CTs have a weak dependence on ϕ.

The ϕ dependence of the absorption spectra for zigzag CTs is further studied, since it is weak for armchair CTs. The electronic states exhibit a periodic oscillation as ϕ varies at $\alpha=0°$. The Aharonov-Bohm (AB) effect is also shown in the optical excitations. The absorption spectra, as shown in Fig. 3(a), show that the separation of each pair of peaks widens with an increase in ϕ. The separation reaches the maximum at $\phi=0.5\ \phi_0$ and recovers to the $\phi=0$ case at $\phi=\phi_0$. The oscillation is symmetric around $\phi=0.5\ \phi_0$ and periodic with a period ϕ_0. The oscillation could be seen also in Fig. 4(a) for the ϕ dependence of the excitation energy (ω_{ex}). When B is perpendicular to the symmetric axis, i.e., $\alpha=90°$, Fig. 3(b) shows that the splitting of absorption peaks is different than that of $\alpha=0°$. In the former, each pair of peaks, at low frequency, has a wider separation as ϕ increases, but it is op-

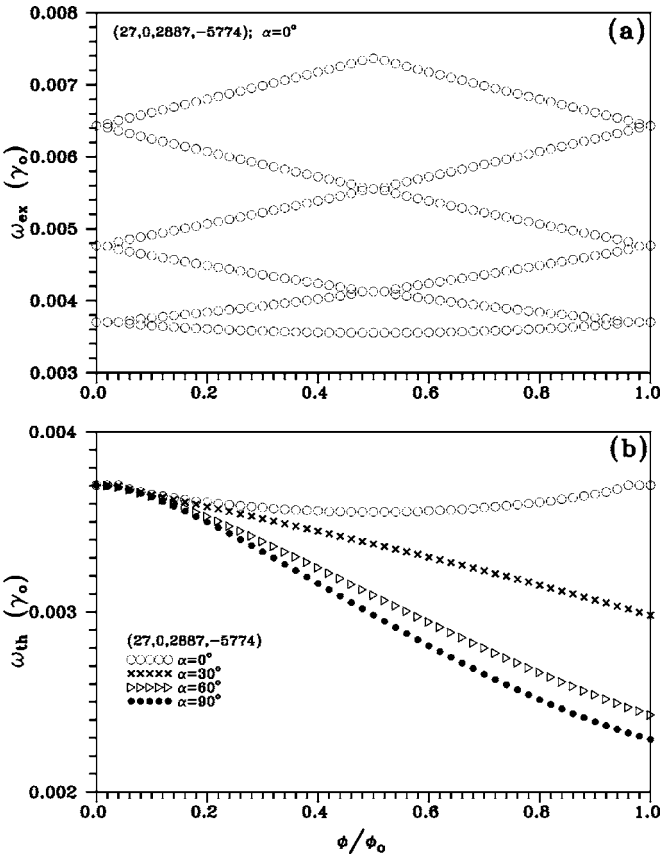

FIG. 4. (a) ϕ-dependent excitation energy at $\alpha=0°$ and (b) ϕ-dependent threshold excitation energy at different α's are calculated for the (27,0,2887, −5774) toroid.

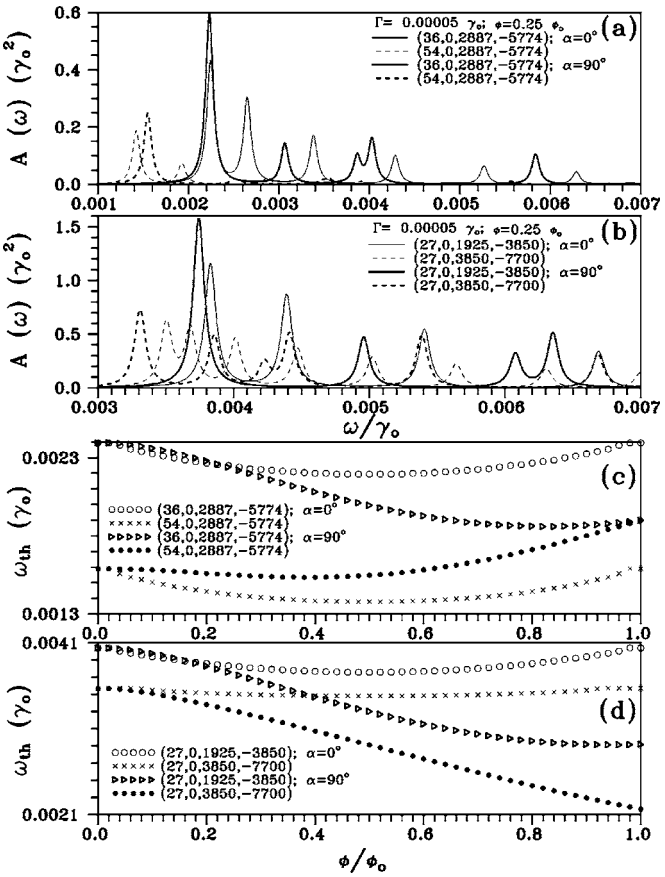

FIG. 5. Absorption spectra of the zigzag toroids are shown at $\alpha=0°$, 90° for (a) different heights and (b) different radii. (c) and (d) are similar plots as in (a) and (b), but shown for the threshold excitation energy.

posite in the latter. Moreover, the splitting of absorption peaks with higher frequency is absent. The reason is that $B_{\|}$ shifts L but $B_{\perp}$ couples different L's. The closer to the Fermi level the state is, the stronger the coupling effect becomes.

At $\alpha=0°$, the excitation energy, which is defined by $\omega_{\mathrm{ex}}=E^{c}(J_a,L+1)-E^{v}(J_a,L)$, varies with increasing ϕ and could also present the AB effect. Figure 4(a) shows that the excitation energy is symmetric around $\phi=0.5\ \phi_0$ and has a period ϕ_0. The oscillatory amplitude for the high-frequency excitation has a stronger ϕ dependence, but the corresponding absorption peak is lower and difficult to observe in experiments. So the threshold excitation energy is more important than others since it has the strongest absorption peak. As $\alpha\neq 0°$, ω_{th} monotonously decreases with an increase in ϕ. Meanwhile, ω_{th} is getting smaller as α increases. The reduction of magnetic flux along the symmetric axis is the main reason.

In order to understand the dependence of magneto-optical excitations on the toroid geometry, the variations in absorption spectra of CTs with different heights and radii are investigated. Since the Coulomb interaction is reduced with increasing toroid height, the smaller excitation energy and lower peak height are expected, as shown in Fig. 5(a), at $\phi=0.25\ \phi_0$ and $\alpha=0°$, 90°. Moreover, the absorption peak of higher CTs decays more rapidly as ω_{ex} increases. Compared with the height dependence, the radius dependence of the absorption spectrum is very different. As the radius increases, there are more allowed L states leading to the increase in transition channels. Thus more absorption peaks occur for a larger CT, as shown in Fig. 5(b). On the other hand, the changes in the excitation energy and the peak height for different radii are smoother than those for different heights. The reason behind the result is the curvature effect has a stronger height dependence, which leads to the obvious changes in excitation energies. As for ω_{th}, at $\alpha=0°$, it is symmetric around $\phi=0.5\ \phi_0$ at $\phi\leqslant\phi_0$ and decreases with increasing toroid height in Fig. 5(c). At $\alpha=90°$, however, ω_{th} monotonously decreases as ϕ increases for the lower CTs, but for the higher CTs, ω_{th} initially declines then slowly grows to a constant in an increase of ϕ, as shown in Fig. 5(c). Concerning the radius-dependent ω_{th} at $\alpha=0°$ [Fig. 5(d)], the change in the magnitude of ω_{th} with increasing radius is smaller than that of ω_{th} for different heights. Figure 5(d) further shows that ω_{th}, at $\alpha=90°$, monotonously decreases as ϕ increases for different radii. In addition, ω_{th} seems to be independent of the toroid radius for the larger CT, e.g., $(27,0,p,-2p)$ CTs for $p\geqslant 2887$. Therefore, the radius dependence of ω_{th} is much weaker than the height dependence.

In conclusion, we have studied the magneto-optical properties of zigzag CTs and armchair CTs. They are significantly affected by the toroid geometry (height, radius, chiral angle),

the magnitude, and the direction of the magnetic field. For the armchair CTs, they only exhibit one prominent absorption peak even in a magnetic field. The position and amplitude of the peak both have a weak dependence on ϕ's and α's. However, the absorption spectra of the zigzag CTs are apparently changed as ϕ or α varies. The excitation energy, at $\alpha=0°$, displays the periodic AB oscillation as ϕ is altered. At $\alpha \neq 0°$, the threshold energy monotonously declines as ϕ increases, and decreases as α grows. Furthermore, ω_{th}, at $\alpha = 90°$, has a very weak ϕ dependence for the higher CT, and it is independent of the toroid radius for the larger CT. The absorption spectra directly reflect the characteristics of the magnetoelectronic states. The optical measurements can be used to verify the predicted absorption spectra.

This work was supported in part by the National Science Council of Taiwan, the Republic of China under Grant No. NSC 93-2112-M-145-001.

[1] S. Iijima, Nature (London) **354**, 56 (1991).
[2] J. Liu, H. Dai, J. H. Hafner, D. T. Colbert, R. E. Smalley, S. J. Tans, and C. Dekker, Nature (London) **385**, 780 (1997).
[3] R. Martel, H. R. Shea, and P. Avouris, Nature (London) **398**, 299 (1999).
[4] B. I. Dunlap, Phys. Rev. B **46**, R1933 (1992).
[5] S. Itoh, S. Ihara, and J. I. Kitakami, Phys. Rev. B **47**, R1703 (1993).
[6] S. Ihara, S. Itoh, and J. I. Kitakami, Phys. Rev. B **47**, 12908 (1993).
[7] S. Itoh and S. Ihara, Phys. Rev. B **48**, 8323 (1993).
[8] S. Itoh and S. Ihara, Phys. Rev. B **49**, 13970 (1994).
[9] M. F. Lin, R. B. Chen, and F. L. Shyu, Solid State Commun. **107**, 227 (1998).
[10] M. F. Lin, and D. S. Chuu, J. Phys. Soc. Jpn. **67**, 259 (1998).
[11] D. H. Oh, J. M. Park, and K. S. Kim, Phys. Rev. B **62**, 1600 (2000).
[12] A. Ceulemans, L. F. Chibotaru, and S. A. Bovin, J. Chem. Phys. **112**, 4271 (2000).
[13] A. Latgé, C. G. Rocha, L. A. L. Wanderley, M. Pacheco, P. Orellana, and Z. Barticevic, Phys. Rev. B **67**, 155413 (2003).
[14] F. L. Shyu, C. C. Tsai, C. P. Chang, R. B. Chen, and M. F. Lin, Carbon **42**, 2879 (2004).
[15] V. Meunier, P. Lambin, and A. A. Lucas, Phys. Rev. B **57**, 14886 (1998).
[16] R. C. Haddon, Nature (London) **388**, 31 (1997).
[17] M. F. Lin, J. Phys. Soc. Jpn. **67**, 1094 (1998).
[18] M. F. Lin and D. S. Chuu, Phys. Rev. B **57**, 6731 (1998).
[19] L. Liu, G. Y. Guo, C. S. Jayanthi, and S. Y. Wu, Phys. Rev. Lett. **88**, 217206 (2002).
[20] S. Latil, S. Roche, and A. Rubio, Phys. Rev. B **67**, 165420 (2003).
[21] C. C. Tsai, F. L. Shyu, C. W. Chiu, C. P. Chang, R. B. Chen, and M. F. Lin, Phys. Rev. B **70**, 075411 (2004).
[22] M. F. Lin, Phys. Rev. B **58**, 3629 (1998).
[23] M. F. Lin, J. Phys. Soc. Jpn. **62**, 2218 (1998).
[24] M. F. Lin, J. Phys. Soc. Jpn. **68**, 1102 (1999).
[25] M. F. Lin, J. Phys. Soc. Jpn. **69**, 3429 (2000).
[26] M. F. Lin, J. Phys. Soc. Jpn. **68**, 3585 (1999).
[27] M. F. Lin, J. Phys. Soc. Jpn. **68**, 3744 (1999).
[28] H. R. Shea, R. Martel, and P. Avouris, Phys. Rev. Lett. **84**, 4441 (2000).
[29] F. L. Shyu, C. P. Chang, R. B. Chen, C. W. Chiu, and M. F. Lin, Phys. Rev. B **67**, 045405 (2003).
[30] J. G. Johnson and G. Dresselhaus, Phys. Rev. B **7**, 2275 (1973).
[31] M. F. Lin, F. L. Shyu, and R. B. Chen, Phys. Rev. B **61**, 14114 (2000).
[32] M. F. Lin, Phys. Rev. B **62**, 13153 (2000).
[33] M. F. Lin and K. W.-K. Shung, J. Phys. Soc. Jpn. **66**, 3294 (1997).
[34] M. F. Lin and Kenneth W.-K. Shung, Phys. Rev. B **50**, R17744 (1994).
[35] F. L. Shyu and M. F. Lin, J. Phys. Soc. Jpn. **71**, 1820 (2002).
[36] A. Jorio, M. A. Pimenta, A. G. S. Filho, G. G. Samsonidze, A. K. Swan, M. S. Unlu, B. B. Goldberg, R. Saito, G. Dresselhaus, and M. S. Dresselhaus, Phys. Rev. Lett. **90**, 107403 (2003).
[37] W. A. de Heer, W. S. Bacsa, A. Chalelain, T. Gerifin, R. Humphrey-Baker, L. Forro, and D. Varget, Science **268**, 845 (1995).
[38] S. M. Bachilo, M. S. Strano, C. Kittrell, R. H. Hauge, R. Smalley, and R. B. Weisman, Science **298**, 2361 (2002).
[39] O. Jost, A. A. Gorbunov, W. Pompe, T. Pichler, R. Friedlein, M. Knupfer, M. Reibold, H. D. Bauer, L. Dunsch, M. S. Golden, and J. Fink, Appl. Phys. Lett. **75**, 2217 (1999).
[40] S. Kazaoui, N. Minami, H. Yamawaki, K. Aoki, H. Kataura, and Y. Achiba, Phys. Rev. B **62**, 1643 (2000).
[41] M. Ichida, S. Mizuno, Y. Tani, Y. Saito, and A. Nakamura, J. Phys. Soc. Jpn. **68**, 3131 (1999).
[42] C. K. Kane, and E. J. Mele, Phys. Rev. Lett. **78**, 1932 (1997).
[43] G. D. Mahan, *Many-Particle Physics* (Plenum, New York, 2000).